

Development of a Hybrid Compressed Gas Engine/PEFC Power System Using the Dissociation Expansion Characteristics of Gas Hydrate

Shin'ya OBARA*

*Power Engineering Laboratory, Department of Electrical and Electronic Engineering, Kitami Institute of Technology
165 Koen-cho, Kitami, Hokkaido 090-8507, Japan
E-mail: obara@mail.kitami-it.ac.jp

Abstract

The pressure of dissociation and expansion of a gas hydrate can fully power a compression gas engine with a temperature change from 0°C to 10°C. The use of green energy (high temperature) and simple refrigeration (low temperature) can easily provide this temperature difference. The dissociation characteristics of a hydrate can be used to develop a clean and efficient hydrate actuator (HA). In this paper, we examine the operation of a hybrid power system consisting of an HA engine and a proton-exchange membrane fuel cell (PEFC), using an example application of an individual house in Sapporo, Japan. A power-generation system that uses the exhaust heat of a PEFC and the cold energy of a heat pump to dissociate and recombine a hydrate is proposed. The results of this analysis indicate that the average electricity production efficiency on a representative day may reach 60.5%. This technique of using the dissociation expansion characteristics of a gas hydrate for power generation deserves further attention in the search for clean energy.

Keywords: Methane hydrate, Hydrate actuator, Hybrid power system, Dissociation, Compressed gas engine, Operation planning

1. Introduction

Hydrates are often present in applications such as the transportation of gaseous fuel and submarine storage of CO₂. For example, Profio et al. [1] evaluated hydrates in hydrogen storage power, while Ersland et al. [2] and Kvamme et al. [3] investigated hydrates in the capacity of submarine storage of carbon dioxide. There are also many cases of study of hydrogen storage technology by a hydrate [4, 5]. One characteristic of a hydrate is that large gas dissociation pressures can result from small temperature changes. For example, if a CO₂ hydrate is heated from 0°C to 10°C, the dissociated gas will pressurize to about 30 atm. This temperature change can be induced using green energy such as sunlight (high temperature) and a refrigerating process (low temperature). The pressure of the dissociation expansion resulting from this process can be used to power a compression gas engine, which can be referred to as a hydrate actuator (HA).

When obtaining heat energy from a fossil fuel, about 30% of the calorific value is lost as exhaust heat at a temperature of 150°C or less. In Japan, the percentage of primary energy that results in this low-temperature exhaust heat exceeds 30%. This low-temperature exhaust heat can be used for space heating but has few other uses. A technique for transforming this exhaust heat into electrical energy would be beneficial. Such power-generation technologies are being actively studied. For instance, an example of exhaust heat recovery of a diesel power plant has been reported by

Bombarda et al. [6]. If a hydrate actuator could be successfully developed, a new means for generating power from exhaust heat could be proposed. The low-temperature and high-temperature heat sources of an HA are about 0°C and 10°C , respectively. Therefore, an HA would perform well in a cold region with access to the outdoor air temperature.

The literature does not currently present the use of the dissociation expansion characteristics of a hydrate as a power source. If successful, this technique may develop into a new field of clean power generation. In this paper, the operation of a hybrid system including an HA generator and a proton-exchange membrane fuel cell (PEFC) is investigated for application as a power-generation system for homes. Because the exhaust heat temperature of PEFC is low, there is little study on this exhaust heat use [7, 8]. We propose an efficient power-generation system that would run on the exhaust heat of a PEFC combined with a heat pump to drive dissociation and recombination in an HA.

2. System Outline

2.1 Dissociation and Recombination Characteristics of Gas Hydrate

Figure 1 shows the temperature-pressure characteristics of various kinds of gas hydrates. This figure was drawn based on the investigation of Sloan and Koh [9]. A gas hydrate changes pressure as the temperature changes, due to gas dissociation. For example, if methane hydrate at 0°C is heated to 10°C , the pressure of the dissociated gas will rise up to about 4 MPa. This pressure differential can operate a compression gas engine. To obtain a pressure difference of 4 MPa by the dissociation and recombination of methane hydrate, temperatures ranging from less than 0°C (supercooling) to more than 10°C (overheating) are actually needed. Because the hydrates of ethane, propane, and carbon dioxide also undergo large pressure changes for small temperature changes, they can also be used to operate a hydrate actuator. Furthermore, the realization of an unprecedented clean power system may be possible by converting the power of an actuator into the turning effort of a dynamo.

2.2 Configuration of a Hydrate Actuator (HA)

Figure 2 shows the configuration for the proposed HA. A hydrate is introduced into two pressurized containers: one column for gas dissociation and one column for the recombined hydrate. In the column for gas dissociation, the hydrate is heated by a heating medium supplied from the outside. In this case, gas in the hydrate dissociates, and the high-pressure gas is supplied to an engine unit (consisting of a cylinder, piston, connecting shaft, and crankshaft). The pressure pushes down the piston of the engine unit. As the piston rises by the inertial force of the flywheel, the gas in the cylinder is discharged to the other column. The hydrate recombines in this column due to cooling supplied from the outside. The engine can be operated by continuously routing the hydrate through the two cylinders and the engine unit. If the number of cylinders is increased, the power of the output shaft is stabilized, but the friction loss from the cylinder piston also increases. In this paper, an engine with only two cylinders is assumed.

The dissociated gas of methane hydrate is used as the working medium of the HA. The actuator shown in Fig. 2 uses the same principle as a compression gas engine. The volume of each hydrate container (the two columns) is dependent on the desired power level, the pressure of the dissociated gas, and the dissociation-recombination rate of the hydrate. It is also dependent on requirements concerning equipment cost and safety.

2.3 Characteristics of an HA Engine

Currently, examples of HA engines are not found in the research literature. There is one example of an actuator using a hydrogen-storing metal alloy (described as an MH engine) using similar technology. Recently, MH actuators were investigated by Lloyd and Kim [10] and Kurosaki et al. [11]. The HA engine shares the following characteristics with the MH engine:

- a. Because the HA engine has a small difference between the dissociation temperature (high temperature) and recombination temperature (low temperature), it would be effective in applications using exhaust heat or green energy.
- b. The gas pressure of the HA engine has a high energy density because the pressure used in the HA is large as compared to that of the MH engine.
- c. Carbon dioxide, methane, ethane, and propane in hydrates have larger molecular masses than hydrogen. Therefore, the working fluids of these gases produce more energy for the same volume flow rate.

These technical issues are also expected in the development of an HA engine:

- a. If the dissociation and recombination rates of a hydrate are slow, the volume of the two columns must be increased.
- b. The storage of high-pressure gas requires safety measures.
- c. Compared to fossil-fuel-based combustion engines, the energy volume density and energy mass density of the HA engine are low.

2.4 Specifications of an HA Engine

In this paper, a power system for homes with power needs of 1 kW is explored. Because the temperature in the cylinder is low compared to engines (the Carnot cycle, Diesel cycle, etc.), exhaust gas losses and cooling losses in the reciprocating-type compression gas engine shown in Fig. 2 are small due to the small difference in temperature between the working fluid and the outdoor air temperature, resulting in little radiation heat transfer. The mechanical losses due to sliding resistance, vibration, etc. in a compression gas engine should be similar to those in a combustion engine. Generally, the maximum thermal efficiency of an Otto-cycle engine is about 30%. Therefore, the thermal efficiency of a compression gas engine is assumed to be 60% by estimating the efficiency of the HA engine twice. To obtain a 1-kW output of brake shaft power in an HA engine, methane at 7 MPa must be supplied to the engine at 0.025 m³/minute, with methane recovered from the engine at 3 MPa. Based on the characteristic dissociation and recombination rates of methane hydrate shown in Fig. 3, the designated rate is set at 400 g/hour. This figure agrees well with the experimental result of Ebinuma and Uchida [12]. The cylinder containing hydrate shown in Fig. 3 has a volume of 1.2 L and undergoes 1500-rpm rotation. On the one hand, when the mode exchange of columns A and B, shown in Fig. 2, occurs every 10 minutes, the recombination and dissociation rates for each column volume are 0.035 m³. On the other hand, if the mode exchange of columns A and B takes place every 30 minutes, two 0.105-m³ columns will be required. However, the volume of these pressurized containers is greatly influenced by the heat transfer control technology used and the dissociation and recombination rates of the hydrate.

2.5 Configuration of the HA Engine and PEFC Hybrid Power-Generation System

Figure 4 shows schematics of an HA engine and PEFC (proton-exchange membrane fuel cell) hybrid power-generation system (HPHS). The HPHS consists of a PEFC subsystem and an HA

subsystem containing an engine unit. The PEFC subsystem contains a reformer, a DC-AC converter, an inverter, and an air heat source heat pump. By supplying natural gas to the reformer, hydrogen is supplied to the PEFC. Power from the fuel cell is supplied to the demand side through the DC-AC converter and the inverter. The exhaust heat of the fuel cell system (heat generation of the cell stack and exhaust heat of the reformer) is supplied to a heating-medium tank in the HA subsystem. The air heat source heat pump is operated by the generator output of the HA subsystem. The high temperature and low temperature of the heat pump are supplied to the heating-medium tank and cooling-medium tank, respectively. A heat exchanger is installed in the heating-medium tank and cooling-medium tank. The heating medium and cooling medium supply a warm temperature and cold temperature to column A and column B, respectively, through flow path control valves. The operating procedure for the HPHS is described below.

3. Operating Method of HPHS

3.1 Power and Heat Load

Figure 5 shows a standard pattern for a power load and heat load in Sapporo, Japan. Figure 5 was reported by Narita in a past study [13]. The HPHS is independently introduced into a standard house in Sapporo exhibiting these load patterns. Therefore, system interconnection with commercial electric power is not used. Because space heating is included in the heat load and there is no need for space cooling, there is no difference in the power load from month to month. However, heat loads differ greatly between summer (July and August) and winter (from December to February). The proposed HPHS shown in Fig. 4 is operated based on the load pattern of Fig. 5 [13]. Because the heat load in winter is very large compared to the power load, it is best to optimize the operation of the system based on the heat load. In contrast, because the difference between the power load and the heat load in the summer is small, it is best to optimize the system management in this case based on the power load, which has a high unit price. Because the exhaust heat in the proposed HPHS is used for the dissociation of the hydrate, heat supplied to the demand side must be supplied from another heat source or must be supplied from the heat pump. To simplify the investigation of this system, this paper assumes that heat is supplied to the demand side from another heat source. In other words, this HPHS is a mono-generation system limited to power generation.

3.2 Operating Method of the System

Generally, the efficiency of the partial-load operation of a reciprocating-type engine is much less than the partial-load operation of a PEFC with a reformer. Therefore, in this paper, the power load pattern of Fig. 5 (a) is divided into a base load (0.2 kW or less) and a change load (0.2 kW). The base load corresponds to the HA engine, and the change load corresponds to the PEFC.

(1) Power of the HA engine

The generator output $E_{g,t}$ of the HA engine is supplied to the base load power and operation of the heat pump included in the PEFC subsystem. Here subscript t expresses the sampling time. The base load $E_{nb,t}$ is 0.2 kW in this paper. The COP (coefficient of performance, $\chi_{h,ot}$ and $\chi_{c,ot}$) values of the warm temperature ($H_{hp,h,t}$) and cold temperature ($H_{hp,c,t}$) of the heat pump are dependent on the outdoor air temperature, ot . Because the power consumption of the heat pump

differs for the warm-temperature standard ($H_{hp,h,t}$) and the cold-temperature standard ($H_{hp,c,t}$), the value of the largest power consumption (Eq. (1) or Eq. (2)) is set as the load.

Standard of cooling

(In the case of $H_{hp,c,t}/\chi_{c,ot} > H_{hp,h,t}/\chi_{h,ot}$)

$$E_{g,t} = (E_{nb,t} + H_{hp,c,t}/\chi_{c,ot})\eta_{iv2} \quad (1)$$

Standard of heating

(In the case of $H_{hp,h,t}/\chi_{h,ot} > H_{hp,c,t}/\chi_{c,ot}$)

$$E_{g,t} = (E_{nb,t} + H_{hp,h,t}/\chi_{h,ot})\eta_{iv2} \quad (2)$$

(2) Power of the PEFC

The power $E_{f,t}$ of the PEFC is calculated using Eq. (3) for the efficiency of the electricity production of a cell stack $E_{nf,t}$, a reformer (η_r), a cell stack (η_f), a DC-AC converter (η_{dc}), and an inverter (1) (η_{iv1}).

$$E_{f,t} = E_{nf,t}/(\eta_r \cdot \eta_f \cdot \eta_{dc} \cdot \eta_{iv1}) = E_{nf,t}/(\eta_{rf} \cdot \eta_{dc} \cdot \eta_{iv1}) \quad (3)$$

Here, the sum total efficiency of the reformer and the cell stack is expressed by η_{rf} ($=\eta_r \cdot \eta_f$). From the calorific value γ and the mass flow rate G_t of the natural gas supplied to the reformer, the heating value $E_{fs,t}$ ($=\gamma \cdot G_t$) supplied to the PEFC subsystem can be calculated. Therefore, Eq. (4) defines the sum total power-generation efficiency η_{rf} of a reformer and a cell stack. Moreover, the reformer efficiency η_r is calculated by Eq. (5) from the calorific value $H_{rg,t}$ of hydrogen contained in the reformed gas of a reformer exit. Here Eq. (6) defines the load factor L_t from the power-generation capacity of the PEFC C_f and $E_{fs,t}$.

$$\eta_{rf} = E_{nf,t}/E_{fs,t} = E_{nf,t}/(\gamma \cdot G_t) \quad (4)$$

$$\eta_r = H_{rg,t}/(\gamma \cdot G_t) \quad (5)$$

$$L_t = (E_{nf,t}/C_f) \cdot 100 \quad (6)$$

Figure 6 (a) shows the experimental results for η_r and L_t , η_{rf} and L_t . Figure 6 shows the characteristics of the PEFC with a reformer used in a past study of Obara [14].

(3) Heat balance

The dissociation heat $H_{d,t}$ of a hydrate is supplied from the exhaust heat $H_{f,t}$ of the PEFC subsystem and the heat of the heat pump $H_{hp,h,t}$. If L_t is determined by the power load $E_{f,t}$ of the PEFC subsystem, the power-generation efficiency η_{rf} of a cell stack with a reformer will be determined by Fig. 6 (a), and the exhaust heat rate η_{eh} will be obtained using Fig. 6 (b). However, the recombination heat $H_{re,t}$ of a hydrate is supplied from the cold temperature $H_{hp,c,t}$ of the heat pump, where $H_{f,t}$ and $H_{hp,h,t}$ and $H_{hp,c,t}$ are supplied to the hydrate in each column through the heating medium and cooling medium, respectively. Equations (7) and (8) are the balance formulas of the warm-temperature heat and cold-temperature heat of the HPHS. The left-hand side of each formula represents the heat supply, and the right-hand side represents the heat demand. The

exhaust heat of the PEFC subsystem and the heat of the heat pump spread to the heating medium and cooling medium. These efficiencies are denoted by η_{hm} and η_{cm} , respectively. The radiation loss in a pipe and the resistance of heat transfer in the heating-medium tank are contained in these efficiencies. The efficiencies $\eta_{loss,d}$ and $\eta_{loss,re}$ are the dissociation and recombination efficiencies of the hydrate, respectively. The losses $\eta_{loss,d}$ and $\eta_{loss,re}$ relate to the radiation of a pipe and the heat transfer resistance of the heat exchangers installed in each column.

Warm-temperature heat

$$H_{f,t} + H_{hp,h,t} + \eta_{hm} \cdot H_{hm,t} = H_{d,t} / \eta_{loss,d} \quad (7)$$

Cold-temperature heat

$$H_{hp,c,t} + \eta_{cm} \cdot H_{cm,t} = H_{re,t} / \eta_{loss,re} \quad (8)$$

(4) Engine unit

The generator output $E_{g,t}$ of an HA engine can be determined from Eq. (9) using the dynamo efficiency η_g , the dissociated gas pressure $P_{d,t}$ of a hydrate, the volume flow rate $V_{d,t}$ of the dissociated gas, and the engine efficiency η_a , where $E_{g,t}$ differs with the column capacities used for dissociation and recombination, the dissociation and recombination rates, and the heat transfer amount supplied to each column. Figure 3 displays the relation between the dissociation and recombination rates of methane hydrate and superheating and supercooling. The value of $E_{g,t}$ is obtained after estimating the heat transfer amount between the heating medium, the cooling medium and the hydrate in each column and determining each column volume.

$$E_{g,t} / \eta_g = \eta_a \cdot P_{d,t} \cdot V_{d,t} \quad (9)$$

4. Analysis Method

4.1 Outline of the HA Subsystem

The pressure of dissociated methane hydrate gas is 7 MPa, and the recombined pressure of the hydrate is 3 MPa (Fig. 1). Therefore, the HA engine operates under a pressure difference of 4 MPa. Table 1 shows the efficiencies of the system structure elements used for analysis. Setting the power ($E_{g,t}$) of inverter (2) of the HA subsystem to 0.2 kW, $P_{d,t}$ is 4.0 MPa. The required rate of dissociated gas in this case is $1.08 \cdot 10^{-4}$ m³/s (0.077 g/s) according to Eq. (9). To operate the HA engine according to the base load shown in Fig. 5 (a), it is necessary to supply the dissociated gas at 4 MPa to the engine unit at a flow rate of $1.08 \cdot 10^{-4}$ m³/s. If the dissociation and recombination rates of methane hydrate are estimated from Fig. 3 as described in Section 2.4, then, when exchanging the mode of each column every 10 minutes, the column capacity is 0.035 m³. The dissociation and recombination rates of methane hydrate given in Fig. 3 are smaller than the demand of dissociated gas in an HA engine operating according to a 0.2-kW base load. Therefore, each column capacity is dependent on the dissociation and recombination rates of the hydrate.

4.2 Analysis Program

(1) Heating value of hydrate dissociation and recombination

The heat of decomposition and the specific heat of methane hydrate are 436.8 J/g and 1.9 J/(g·K), respectively. From the flow demand of the dissociated gas (described in Section 4.1), the efficiencies

$\eta_{loss,d}$ and $\eta_{loss,re}$, the heat of dissociation $H_{d,t}$ and the heat of recombination $H_{re,t}$ of the hydrate can all be obtained by the following formulas.

$$H_{d,t} = 0.077 \cdot \{436.8 + 1.9 \cdot (T_{sh} - T_{hd,t})\} \eta_{loss,d} \quad (10)$$

$$H_{re,t} = 0.077 \cdot \{436.8 + 1.9 \cdot (T_{hr,t} - T_{sc})\} \eta_{loss,re} \quad (11)$$

Here, T_{sh} and T_{sc} are the superheating and supercooling temperatures at the time of dissociation and recombination of the hydrate, respectively. In this paper, the temperatures of dissociation and recombination are 0 °C and 10 °C, respectively. In this case, the supplied temperatures to each column are set at -5 °C and 15 °C, respectively. Consequently, the amount of superheating and supercooling is 5 °C.

(2) Power of the PEFC subsystem

If the power load ($E_{f,t}$) of the PEFC subsystem is known, the demand production of electricity $E_{nf,t}$ of a cell stack can be determined by Eq. (3). The value for η_{rf} in Eq. (3) can be obtained from Eqs. (4) to (6) and Fig. 6 (a). Values from Table 1 are used for η_{dc} and η_{ivl} in Eq. (3).

(3) Input and output of the heat pump

The COP ($\chi_{h,ot}$ and $\chi_{c,ot}$) of the heat pump is affected by the outdoor air temperature ot [°C]. In this analysis, $\chi_{h,ot} = \chi_{c,ot} = 3.0$ is assumed, based on a fixed temperature ot . The heating load $H_{hp,h,t}$ and cooling load $H_{hp,c,t}$ of the heat pump are calculated by introducing Eqs. (10) and (11) into Eqs. (7) and (8). The power consumptions $E_{hp,h,t}$ and $E_{hp,c,t}$ of the heat pump are obtained from the following formulas, contained in Eqs. (1) and (2).

$$E_{hp,h,t} = H_{hp,h,t} / \chi_{h,ot} \quad (12)$$

$$E_{hp,c,t} = H_{hp,c,t} / \chi_{c,ot} \quad (13)$$

When there is a difference between $E_{hp,h,t}$ and $E_{hp,c,t}$, the magnitudes of $E_{hp,h,t}$ and $E_{hp,c,t}$ are compared, and the larger value is taken as the load of the dynamo.

5. Example Results

The operation plan of the proposed HPHS described in Fig. 4 was investigated using a power load pattern (Fig. 5 (a)) based on a representative day in Sapporo, Japan. These results are described below.

5.1 Power Output of the Subsystem

Figure 7 (a) shows the power output of the PEFC subsystem ($E_{f,t}$) and the HA subsystem ($E_{g,t}$). These power levels are based on the change load and base load of the power load pattern shown in Fig. 5 (a). Figure 7 (b) shows the analysis results of the load factor (L_r) of the PEFC and the PEFC efficiency (η_{rf}) with a reformer. The fluctuation range of the load factor of the PEFC shown in Fig. 7 (b) is 10% to 100%. However, the range of fluctuation of the efficiency η_{rf} of the PEFC with a

reformer for a large change of L_t is small, from 26.5% to 31%, because changes in η_{rf} are small even if L_t changes greatly, as shown in Fig. 6 (a).

5.2 Power Consumption of the Heat Pump

Figure 7 (c) shows the exhaust heat power ($H_{f,t}$) of the PEFC subsystem and the calculation results of the heat ($H_{d,t}, H_{re,t}$) used for the dissociation and recombination of a hydrate. The power consumption of the heat pump ($E_{hp,h,t}, E_{hp,c,t}$) required in this case is also shown in the same figure. The absolute value of the heat used for dissociation and recombination of the hydrate is the same ($H_{d,t} = H_{re,t}$). However, because the dissociation mode can use the exhaust heat of the PEFC subsystem, operation of the heat pump is mainly used for cooling the hydrate (recombination mode). Moreover, the exhaust heat of the PEFC subsystem exceeds the heat used for dissociation of the hydrate during the sampling time ($H_{f,t} > H_{d,t}$). When the COP is 3, the power consumption of the heat pump $E_{hp,c,t}$ is about 14 W. This power is added to the HA engine as a load.

5.3 Fuel Consumption and Power-Generation Efficiency of the HPHS System

Figure 8 (a) shows the analysis results of the natural gas consumption of the proposed HPHS and a PEFC-independent system. Here the PEFC-independent system is a configuration that excludes the heat pump of the PEFC subsystem shown in Fig. 4. The natural gas consumption of the HPHS on a representative day is 44.2% of the PEFC-independent system consumption.

Figure 8 (b) illustrates the analysis results of the power-generation efficiency of the HPHS. When the exhaust heat of the fuel cell system and the heat of the heat pump are used for the dissociation and recombination of methane hydrate, a high power-generation efficiency can be obtained. The average power-generation efficiency on a representative day is 60.5%. As a result of this expected high power-generation efficiency, the proposed HPHS is very attractive as a power-generation system. The next step in this research is to evaluate a trial system for determining the actual power-generation efficiency.

6. Conclusions

The dissociation expansion characteristics of a gas hydrate were used to analyze the operation of a hybrid power system (HPHS) consisting of a methane hydrate HA engine and a proton-exchange membrane fuel cell (PEFC). The power consumption of the heat pump, fuel consumption, power-generation efficiency, etc., were analyzed for the example case of an HPHS used in an individual house in Sapporo, Japan. The power load pattern on a representative day was divided into a base load of 0.2 kW or less and a fluctuating load exceeding 0.2 kW. The HA engine and PEFC were applied such that they corresponded to the base load and the fluctuation load. As a result, the following conclusions were obtained:

- (1) The fuel consumption (natural gas consumption) of the HPHS on a representative day is 44.2% of the PEFC-independent system consumption.
- (2) Although the electric power consumption of the heat pump is added as a load on the HA engine, dissociation of the hydrate can be fully accomplished by the exhaust heat of a PEFC system. Therefore, the heat pump is used for cooling the hydrate (recombination mode). The power consumption of a heat pump of COP=3.0 is about 14 W.
- (3) High power-generation efficiency can be obtained by using the exhaust heat of a fuel cell system and the heat of a heat pump for the dissociation and recombination of a hydrate. The

average power-generation efficiency of the HPHS on a representative day would be 60.5%, which is relatively high for an energy system.

A trial production and evaluation of the HPHS are recommended. The proposed HPHS is very promising as a clean energy system.

Nomenclature

E	:	Power [W]
C_f	:	Power-generation capacity of the PEFC subsystem [W]
G	:	Mass flow rate of natural gas [g/s]
H	:	Heat [W]
L	:	Load factor [%]
P	:	Pressure [Pa]
T	:	Temperature [°C]
V	:	Volumetric flow [m ³ /s]

Greek characters

χ	:	COP (coefficient of performance)
γ	:	Calorific value of natural gas [J/g]
η	:	Efficiency [%]

Subscripts

a	:	Actuator engine
c	:	Cooling
cm	:	Cooling of heat medium
d	:	Dissociation of gas hydrate
dc	:	DC-AC converter
eh	:	Exhaust heat of PEFC with reformer
f	:	PEFC subsystem
fs	:	Supply to the PEFC subsystem
g	:	Generator
h	:	Heat
hd	:	Temperature of hydrate under dissociation
hm	:	Heating of heat medium
hr	:	Temperature of hydrate for recombination
hp	:	Heat pump
$iv1, iv2$:	Inverter
nb	:	Base load
nf	:	Fuel cell stack
ot	:	Outside air temperature [°C]
r	:	Reformer
re	:	Recombination of gas hydrate
rf	:	Fuel cell with reformer
rg	:	Calorific value of hydrogen [J/g]

<i>sc</i>	:	Supercooling
<i>sh</i>	:	Superheating
<i>t</i>	:	Sampling time [hour]

Acknowledgement

This work was partially supported by a Grant-in-Aid for Iwatani Naoji Kinen Zaidan 2010.

References

- [1] P. D. Profio, S. Arca, F. Rossi, M. Filippini, Comparison of hydrogen hydrates with existing hydrogen storage technologies: Energetic and economic evaluations, *Int. J. Hydrogen Energy* 34 (22) (2009), 9173-9180.
- [2] G. Ersland, J. Husebø, A. Graue, B. Kvamme, Transport and storage of CO₂ in natural gas hydrate reservoirs, *Energy Procedia*. 1 (1) (2009), 3477-3484.
- [3] B. Kvamme, A. Graue, T. Buanes, T. Kuznetsova, G. Ersland, Storage of CO₂ in natural gas hydrate reservoirs and the effect of hydrate as an extra sealing in cold aquifers, *Int. J. Greenhouse Gas Control*. 1 (2) (2007), 236-246.
- [4] P. D. Profio, S. Arca, F. Rossi and M. Filippini, Claudio Pietra, Comparison of hydrogen hydrates with existing hydrogen storage technologies: energetic and economic evaluations, *Int J Hydrogen Energy*. 34 (22) (2009), 9173-9180.
- [5] A. Talyzin, Feasibility of H₂-THF-H₂O clathrate hydrates for hydrogen storage applications, *Int J Hydrogen Energy*. 33 (1) (2008), 111-115.
- [6] P. Bombarda, C. M. Invernizzi, Claudio Pietra, Heat recovery from diesel engines: A thermodynamic comparison between Kalina and ORC cycles, *Applied Thermal Eng.* 30 (2-3) (2010), 212-219.
- [7] S. Obara, I. Tanno, S. Kito, A. Hoshi, S. Sasaki, Exergy analysis of the woody biomass stirling engine and PEM-FC combined system with exhaust heat reforming, *Int J Hydrogen Energy*. 33 (9) (2008), 2289-2299.
- [8] H. Aki, S. Yamamoto, J. Kondoh, T. Maeda, H. Yamaguchi, A. Murata, I. Ishii, Fuel cells and energy networks of electricity, heat, and hydrogen in residential areas, *Int J Hydrogen Energy*. 31 (8) (2006), 967-980.
- [9] E. D. Sloan, C. A. Koh, *Clathrate Hydrates of Natural Gases*, third ed., CRC Press, New York, 2007.
- [10] G. M. Lloyd, K. J. Kim, Smart hydrogen/metal hydride actuator, *Int J Hydrogen Energy*. 32 (2) (2007), 247-255.
- [11] K. Kurosaki, T. Maruyama, K. Takahashi, H. Muta, M. Uno, S. Yamanaka, Design and development of MH actuator system, *Sensors and Actuators A: Physical*. 113 (1) (2004), 118-123.
- [12] T. Ebinuma, T. Uchida., Study on a recombined-dissociation process for gas-hydrate Utilization, Hokkaido National Industrial Research Institute 2010, <http://www.hniri.go.jp/chap3/pdf99.files/ghkine.pdf>. (2010). (in Japanese)
- [13] K. Narita, The Research on Unused Energy of the Cold Region City and Utilization for the District Heat and Cooling, Ph. D. thesis, Hokkaido University, Sapporo, 1996.

[14] S. Obara, Amount of CO₂ discharged from compound micro-grid of hydrogenation city-gas engine and proton exchange membrane fuel cell, J. Environment and Engineering. 2 (2) (2007), 347-358.

Captions

Table 1 Efficiency of HPHS elements

Fig. 1 Temperature-pressure characteristics of various hydrates

Fig. 2 Hydrate actuator (HA engine)

Fig. 3 Relation between the generation rate of methane hydrate and supercooling temperature. Cylinder, 0.0012 m³, 1500 rpm. [8]

Fig. 4 Configuration of the HA engine and PEFC hybrid power system (HPHS)

Fig. 5 Energy load of an individual house in Sapporo [9]

Fig. 6 Performance of the reforming unit and the PEFC subsystem [10]

(a) Efficiency of the reformer and a PEFC with reformer

(b) Exhaust heat output ratio of a PEFC with reformer

Fig. 7 Analysis results

(a) Generated power

(b) Load factor and efficiency of the PEFC

(c) Power consumption of the heat pump

Fig. 8 Performance of HPHS

(a) Consumption of natural gas

(b) Total power-generation efficiency of proposed HPHS

Table 1 Efficiency of HPHS elements

Inverter (1) η_{iv1}	95 %	Reformer η_r	Fig. 6 (a)
Inverter (2) η_{iv2}	95 %	PEFC with reformer η_{rf}	Fig. 6 (b)
DC-AC converter η_{dc}	95 %	Dissociation $\eta_{loss,d}$	90 %
Generator η_g	90 %	Recombined $\eta_{loss,r}$	90 %
Engine unit η_a	60 %		

Fig. 1 Temperature-pressure characteristics of various hydrates

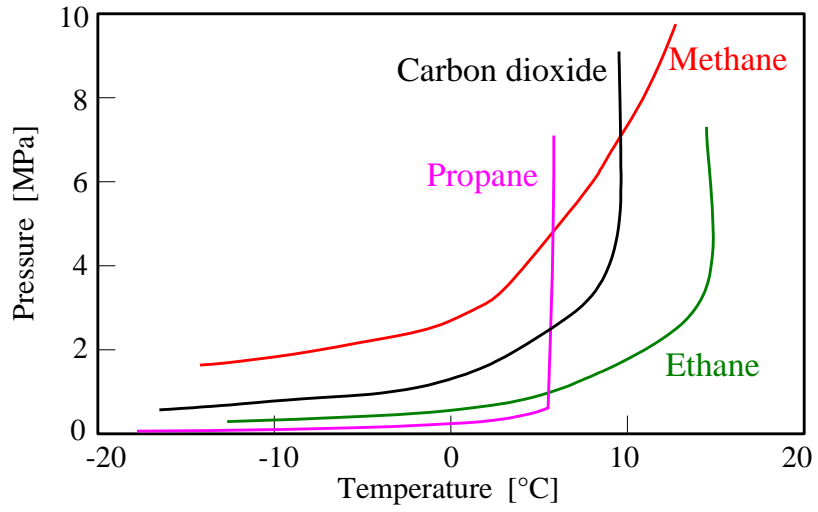


Fig. 2 Hydrate actuator (HA engine)

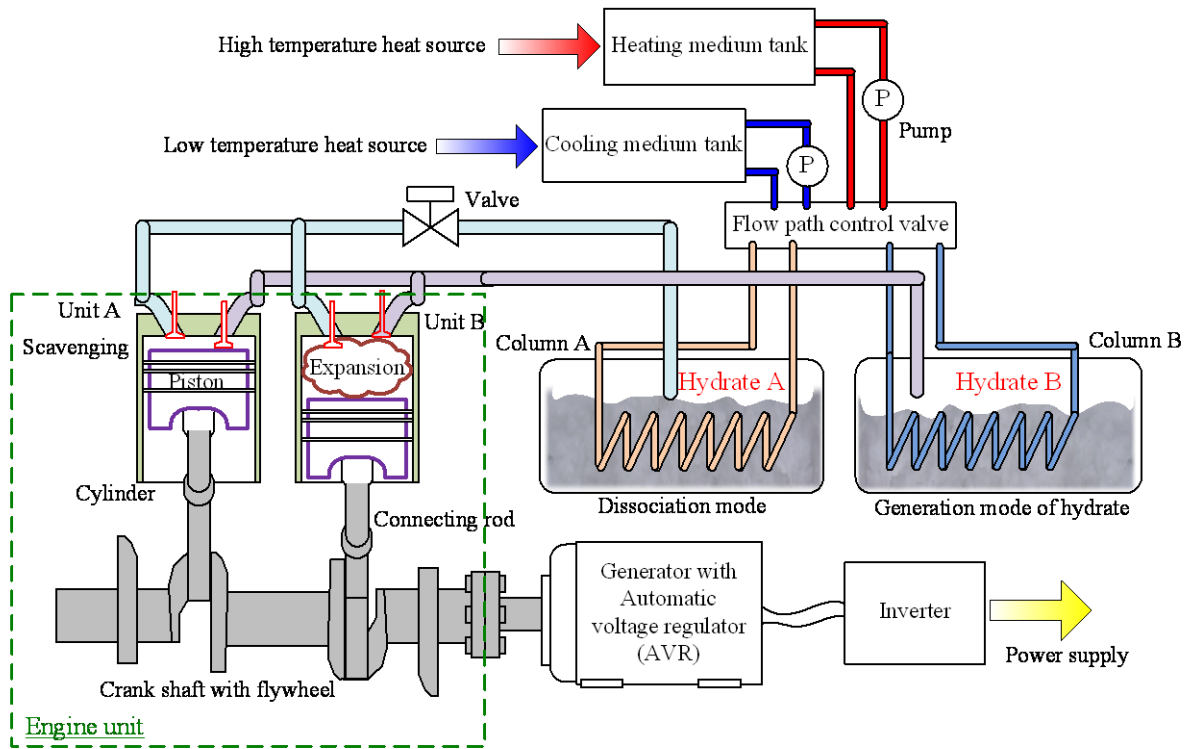


Fig. 3 Relation between the generation rate of methane hydrate and supercooling temperature.
Cylinder, 0.0012 m³, 1500 rpm. [8]

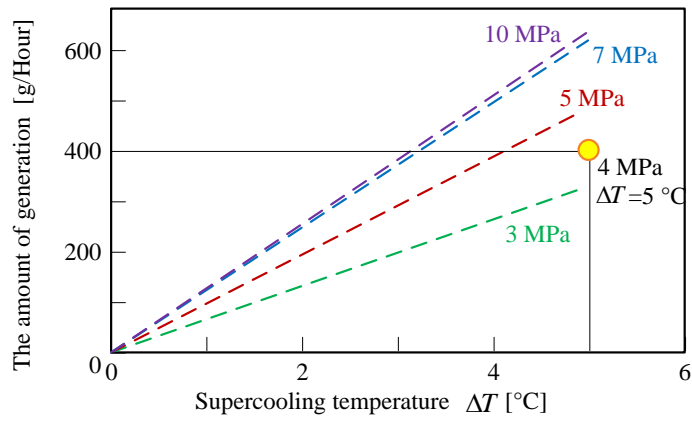


Fig. 4 Configuration of the HA engine and PEFC hybrid power system (HPHS)

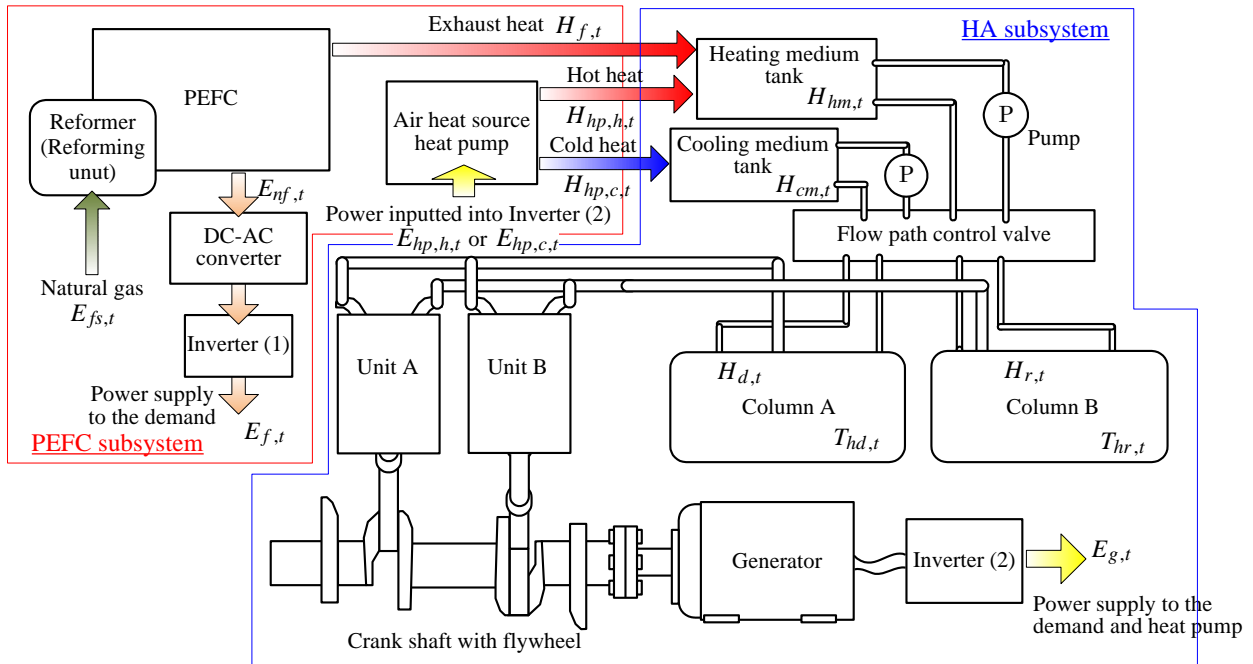
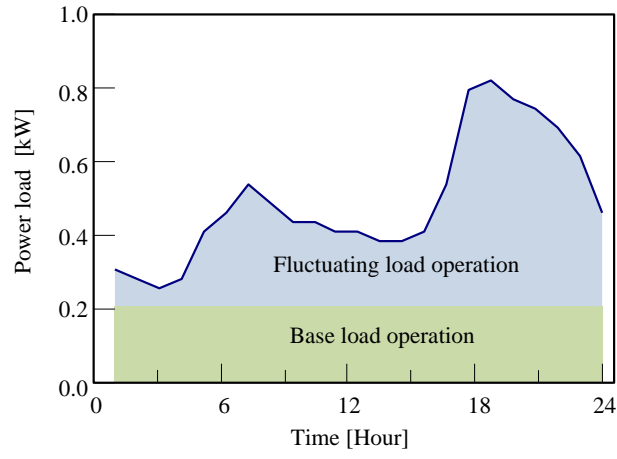


Fig. 5 Energy load of an individual house in Sapporo [9]

(a) Power



(b) Heat

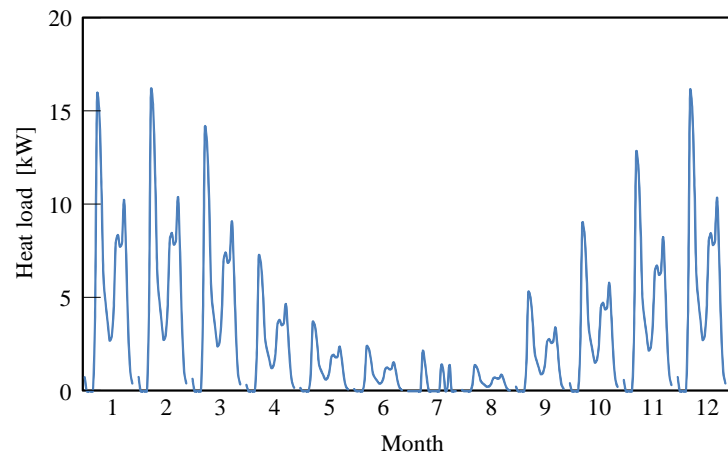
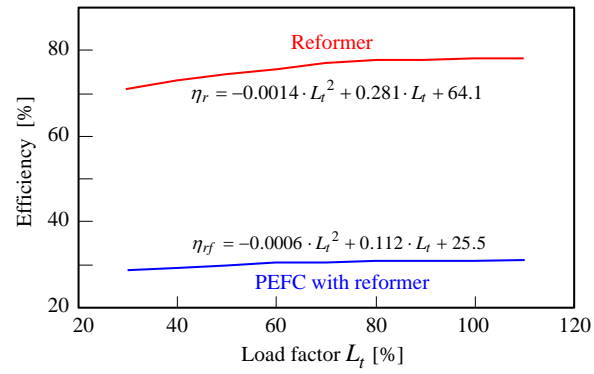


Fig. 6 Performance of the reforming unit and the PEFC subsystem [10]

(a) Efficiency of the reformer and a PEFC with reformer



(b) Exhaust heat output ratio of a PEFC with reformer

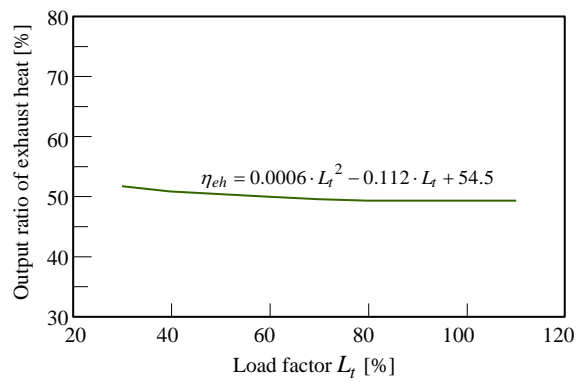
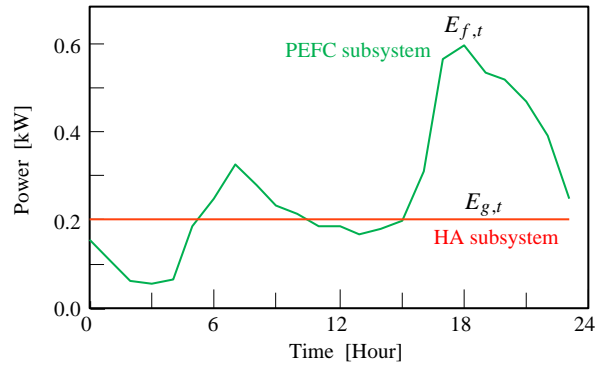
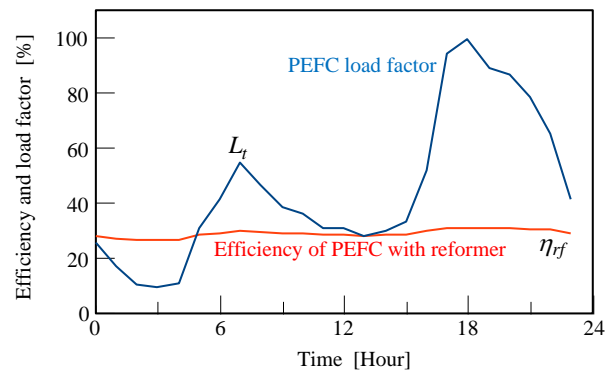


Fig. 7 Analysis results

(a) Generated power



(b) Load factor and efficiency of the PEFC



(c) Power consumption of the heat pump

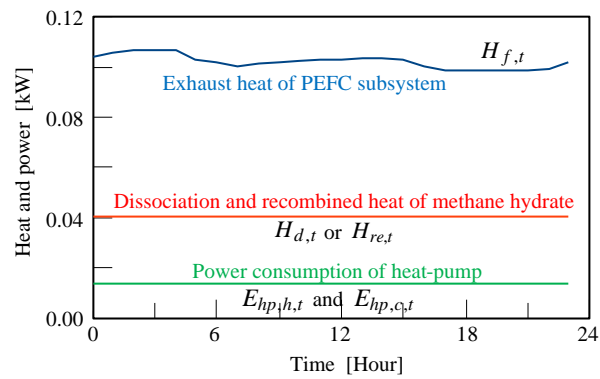
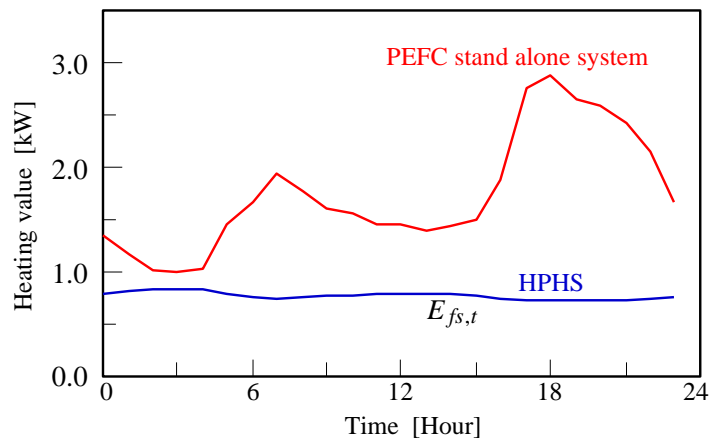


Fig. 8 Performance of HPHS

(a) Consumption of natural gas



(b) Total power-generation efficiency of proposed HPHS

